HHS Public Access

Author manuscript

Acta Biomater. Author manuscript; available in PMC 2019 July 15.

Published in final edited form as:

Acta Biomater. 2018 July 15; 75: 105–114. doi:10.1016/j.actbio.2018.06.007.

RNA Interfering Molecule Delivery from *in situ* Forming Biodegradable Hydrogels for Enhancement of Bone Formation in Rat Calvarial Bone Defects

Minh K. Nguyen[a,†], **Oju Jeon**[a,†], **Phuong N. Dang**[a], **Cong T. Huynh**[a], **Davood Varghai**[b], **Hooman Riazi**[b], **Alexandra McMillan**[a], **Samuel Herberg**[a], and **Eben Alsberg**[a,c,*]

[a]Departments of Biomedical Engineering

[b]Neurological Surgery

[c]Orthopaedic Surgery, Case Western Reserve University, Cleveland, OH

Abstract

RNA interference (RNAi) may be an effective and valuable tool for promoting the growth of functional tissue, as short interfering RNA (siRNA) and microRNA (miRNA) can block the expression of genes that have negative effects on tissue regeneration. Our group has recently reported that the localized and sustained presentation of siRNA against noggin (siNoggin) and miRNA-20a from *in situ* forming poly(ethylene glycol) (PEG) hydrogels enhanced osteogenic differentiation of encapsulated human bone marrow-derived mesenchymal stem cells (hMSCs). Here, the capacity of the hydrogel system to accelerate bone formation in a rat calvarial bone defect model is presented. After 12 weeks post-implantation, the hydrogels containing encapsulated hMSCs and miRNA-20a resulted in more bone formation in the defects than the hydrogels containing hMSCs without siRNA or with negative control siRNA. This localized and sustained RNA interfering molecule delivery system may provide an excellent platform for healing bony defects and other tissues.

Graphical Abstract

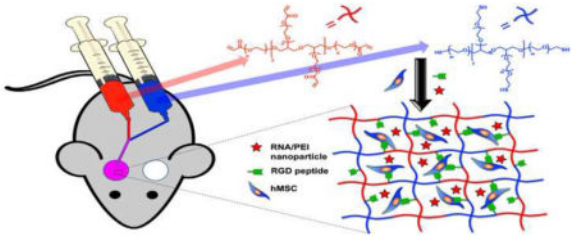

Keywords

RNAi; hydrogel; hMSC; bone regeneration

*Corresponding Author: Professor Eben Alsberg, Case Western Reserve University, eben.alsberg@case.edu.

†Both authors contributed equally in this work

1. Introduction

There is substantial need for strategies to heal bone defects caused by trauma, tumor resection, infection, congenital malformation and degeneration [1]. Current clinical treatments for these defects include autologous, allogeneic and synthetic bone grafts [2, 3]. Although autologous bone grafts are considered the gold standard for bone regeneration, they are often limited by supply and donor-site morbidity [2]. Allografts can be used, but there is potential for immunogenicity and disease transfer [2]. Inorganic materials, such as those composed of hydroxyapatite, may poorly integrate with host tissue or exhibit minimal and/or slow degradation in the body, limiting new bone formation [3–6].

Bone tissue engineering strategies that use mesenchymal stem cells (MSCs), biomaterial scaffolds and/or bioactive molecules offer promise in addressing the shortcomings of current clinical bone grafts [7–10]. hMSCs are an attractive cell source as they can be easily obtained from bone marrow aspirates. hMSCs can expanded substantially while maintaining their capacity to differentiate down multiple cell lineages into, for example, osteoblasts, chondrocytes, adipocytes and myoblasts [11], following subsequent induction via instructive cues such as cytokines. Bone morphogenetic proteins (BMPs), the most potent osteoinductive cytokines, have been extensively investigated for bone tissue engineering [12, 13]. However, these cytokines have a short systemic half live in vivo [14], and supraphysiological amounts are often required due to their rapid degradation and clearance to promote an osteogenic effect, which may lead to ectopic bone formation and potential long-term complications [15]. Sustained presentation of these cytokines may be necessary to achieve adequate rate and quality of bone healing, but controlled delivery from a biomaterial scaffold over a prolonged period of time can be challenging [15, 16].

In addition to growth factors, genetic molecules such as DNA, short interfering RNA (siRNA) and microRNA (miRNA), are useful for engineering bone tissue, as they can regulate gene expression at the transcriptional or post-transcriptional levels. For example, plasmid DNA encoding for BMP-2 has been shown to upregulate hMSC osteogenesis via the production of this protein [17]. Additionally, plasmid DNA inducing BMP-4 production accelerated bone formation in rat calvarial bone defects [18]. Alternatively, siRNAs against BMP antagonists noggin (siNoggin) and chordin (siChordin), for example, inhibited noggin and chordin gene expression, respectively, leading to enhanced osteogenic differentiation of hMSCs [19, 20]. Although the use of plasmid DNA to elicit the production of a specific protein [17, 21] is promising in bone tissue engineering, DNA must be transported into the cell nucleus before transcription of mRNA and subsequent translation of encoded protein can occur [22]. Moreover, delivered sequences of DNA can potentially integrate into the host DNA, which can cause unwanted genetic changes, and production of encoded protein via DNA delivery can only occur in dividing cells [23]. In contrast, siRNA and miRNA need only to be delivered to the cytoplasm where they regulate gene expression post-transcriptionally in both dividing and non-dividing cells [23], and thus they provide a simple, effective alternative technology for promoting tissue formation.

Nano- and microparticles have been utilized to deliver siRNA and miRNA, but it is challenging to target RNA to specific tissues and it is vulnerable to rapid clearance once *in*

vivo [24, 25]. Alternatively, larger three-dimensional (3D) biomaterial matrices such as porous scaffolds [26], electrospun nanofibers [27, 28] and hydrogels [20, 29–32], have been engineered for localized, sustained delivery of RNA molecules. While solid scaffolds and nanofibers permit release of these RNA interfering molecules only to surrounding cell populations, hydrogels, 3D crosslinked hydrophilic polymer networks, have been shown to permit presentation of these RNAi molecules to encapsulated and/or surrounding cells and inhibit expression of targeted genes [20, 29–31]. Recently, we have demonstrated that prolonged suppression of noggin, a BMP-2 antagonist, [33] and/or PPAR-γ, a negative regulator of BMP-mediated osteogenesis [34], via localized, sustained delivery of siNoggin and/or miRNA-20a to hMSCs encapsulated within *in situ* forming poly(ethylene glycol) (PEG) hydrogels increased their osteogenic differentiation *in vitro* [20]. In this work, the hydrogel system's capacity to regenerate bone in full-thickness cranial rat defects was examined to demonstrate its translational potential. Recently, a few hydrogels [35–37] or solid scaffolds [38] have been developed for RNAs delivery to regenerate bone tissue; however, these systems were only investigated for either controlled RNA delivery without cell encapsulation [36, 38] or cell encapsulation without controlled RNA release [35]. Here, for the first time we present an *in situ* forming hydrogel system for both controlled RNA delivery and cell encapsulation to regenerate bone in a rat calvarial bone defect model. Since *in situ* forming hydrogels are considered can be delivered in a minimally invasive manner and easily take the form of complex 3D shapes [39], the hydrogels developed in this study may be advantageous for filling of defects compared to premade solid scaffolds and nanofibers.

2. Materials and methods

2.1. Polymer synthesis

8-arm-PEG-A was synthesized by conjugating acryloyl chloride (Sigma, St. Louis, MO) to the hydroxyl groups of 8-arm-PEG-OH (10 kDa, JenKem Technology USA, Allen, TX) in the presence of triethylamine (TEA, Sigma), as previously described [20]. 8-arm-PEG-A was collected by precipitating the reaction into a 2:1 mixture of diethyl ether/hexane. The polymer was then hydrated in ultrapure pure deionized water (diH_2O) followed by dialysis against diH_2O using a 3,500 Da cutoff membrane for 3 days at 4 °C. diH_2O was changed three times per day. The dialyzed solution was frozen and lyophilized until dry, and the resulting polymer was characterized via ^{1}H NMR.

2.2 Cell isolation and culture

To isolate hMSCs, bone marrow aspirates were obtained from the posterior iliac crest of a healthy twenty three-year old male donor under a protocol approved by the University Hospitals of Cleveland Institutional Review Board. The aspirates were washed with growth medium comprised of low-glucose Dulbecco's Modified Eagle's Medium (DMEM-LG, Sigma) with 10 % prescreened fetal bovine serum (FBS, Gibco). Mononuclear cells were isolated by centrifugation in a Percoll (Sigma) density gradient and the isolated cells were plated at 1.8×10^5 cells/cm^2 in DMEM-LG containing 10 % FBS and 1 % penicillin/streptomycin (P/S, Thermo Fisher Scientific) in a humidified incubator at 37 °C and 5 % CO_2. After 4 days of incubation, non-adherent cells were removed and adherent cell were

maintained in DMEM-LG containing 10 % FBS and 1 % P/S with media changes every 3 days. After 14 days of culture, the cells were passaged at a density of 5×10^3 cells/cm^2. hMSCs were expanded in growth media consisting of DMEM-LG with 10 % FBS (Sigma), 1 % P/S and 10 ng/ml FGF-2 (R&D).

2.3. Hydrogel formation

In situ forming PEG hydrogels were synthesized as previously described [20] with slight modification. Specifically, GRGDSPC peptide (5 mg peptide per g combined PEG) was mixed with 500 μl 8-arm-PEG-A (15 w/v% in phosphate buffered saline (PBS)) for 1 h at room temperature before combining with 500 μl 8-arm-PEG-SH (10 kDa, 96.4% thiolation, JenKem Technology USA) (15 w/v% in PBS), and the 1 ml PEG solution was placed between two glass plates separated by two 0.75 cm spacers. After 30 min, the top plate was removed, and hydrogel discs (5 mm in diameter and 0.75 mm in thickness) were created using a biopsy punch. Hydrogels containing encapsulated hMSCs and RNA were prepared as described above, with hMSCs (passage 3, 10×10^6 cells/ml), BMP-2 (1 μg/implant, Department of Developmental Biology, University of Würzburg, Germany) and/or RNA/PEI complexes (40 μg siRNA/ml) suspended in the PEG macromer solutions prior to crosslinking. siNoggin (5′-AAC ACU UAC ACU CGG AAA UGA UGG G-3′), miRNA-20a (5′-UAA AGU GCU UAU AGU GCA GGU AG-3′) and siNC (5′-UUC UCC GAA CGU GUC ACG UTT-3′) were purchased from Insight Genomics, Falls Church, VA.

2.4. Rat calvarial defect model

The surgical procedures used in this study were conducted according to a protocol approved by the Institutional Animal Care and Usage Committee of Case Western Reserve University which adhered to the National Institute of Health Guide for the Care and Use of Laboratory Animals. Healthy 12-week old male athymic rats (Taconic Biosciences, Hudson, NY) were used for the calvarial defect model. The rats were anesthetized with a ketamine (40–45 mg/kg)/dexemedetomide (0.1–0.15 mg/kg) cocktail via intraperitoneal (IP) injection. Isoflurane (1–3%) was used to maintain the anesthesia during surgery. Bilateral full thickness circular defects (5 mm) were created using a hand drill on both sides of the sagittal suture without harming the dura matter. PEG hydrogels containing encapsulated hMSCs, BMP-2 and/or siRNA were implanted into the defects with the following experimental groups: hydrogel + hMSCs (group 1 or G1), hydrogel + hMSCs + BMP-2 (G2), hydrogel + hMSCs + BMP-2 + negative control siRNA (G3), hydrogel + hMSCs + BMP-2 + siNoggin (G4), hydrogel + hMSCs + BMP-2 + miRNA20a (G5), and hydrogel + hMSCs + BMP-2 + siNoggin + miRNA20a (G6) (Table 1). Hydrogels that did not contain siNoggin and/or miRNA-20a served as controls (G1–3). Each disc-shaped hydrogel contained hMSCs (170,000 cells), BMP-2 (1μg) and/or RNA (0.68 μg). After surgery, the periosteum and skin were closed with 6.0 and 5.0 vicryl sutures (Fisher Scientific), respectively. The rats were then administered atipamezole (1 mg/kg) for reversal of the sedative and analgesic effects of dexemedetomide, and buprenorphine (2 mg/kg) for pain control. After 2 or 12 weeks, the rats were euthanized with carbon dioxide followed by skull explantation. A total of 40 rats were used for a total of 80 defects. Hydrogel constructs of G1 (N=13), G2 (N=14) and G3 (N=13) were implanted into the left side calvarial defects, and hydrogel constructs of G4 (N=13), G5 (N=13), G6 (N=14) were implanted into the right side calvarial defects.

Constructs from each left side group (i.e., G1, G2, and G3) were randomly paired at least 4 times with constructs from each right side group (i.e., G4, G5, and G6). However, one sample from G3, G4 and G6, two samples from G5 and three samples from G2 were lost after four rats died after surgery.

2.5. Biochemical analysis

Two weeks post-implantation, half of the rats were euthanized and the explanted hydrogels were cut into two equal-sized halves. One half of each gel was used for biochemical analysis and the other half for RNA isolation. Each hydrogel for biochemical analysis was homogenized in 1 ml CelLytic M reagent (Sigma) at 35,000 rpm for 60 s using a TH mechanical homogenizer (Omni International, Marietta, GA). The homogenized solutions were centrifuged at 500 g using a Sorvall Legend RT Plus Centrifuge (Thermo Fisher Scientific), and the supernatants (N=6 per group) were then used to quantify alkaline phosphatase (ALP) activity and DNA content. ALP activity was measured by adding 100 μl p-nitrophenyl phosphate (pNPP, Sigma) to 100 μl supernatant in a clear 96 well plate. The mixture was incubate at 37 °C for 30 min, and then the reaction was stopped by the addition of 0.1N NaOH (50 μl) followed by absorbance measurement at 405 nm with a plate reader (VersaMax, Molecular Devices, Sunnyvale, CA). p-nitrophenol (Sigma) with diluted concentrations ranging from 0–0.5 mM was used to make the standard curve [40]. DNA was quantified using a DNA Picogreen assay (Invitrogen) kit according to the manufacturer's instructions. Picogreen reagent (100 μl) was mixed with the supernatant (100 μl) in a black 96-well plate, and the mixture was read on a plate reader set at excitation 485/emission 538. Calcium content of the explanted constructs was measured using a calcium assay kit (Pointe Scientific, Canton, MI) according to the manufacturer's instructions. Specifically, after measuring ALP and DNA content, HCl 1.2 N (600 μl) was then added to the leftover supernatants with homogenized hydrogels (600 μl), and the mixture was placed in a fridge over night and then centrifuged at 500 g. 4 μl of the new supernatant was added to a mixture of color and buffer reagents in a clear 96-well plate, and then the plate was immediately read at 570 nm. ALP activity and calcium content were normalized to DNA content.

2.6. RNA isolation and real-time quantitative reverse transcription-polymerase chain reaction (qRT-PCR)

The other halves of the explanted constructs at the 2 week time point (N=6 per group) were placed in 1ml TRI reagent (Sigma) and homogenized at 35,000 rpm for 60 s using a TH homogenizer (Omni International). The homogenized solution was then centrifuged at 12,000 g for 15 min using a microcentrifuge (accuSpin Micro 17R, Fisher Scientific), and then RNA was isolated according to the manufacturer's instructions. Isolated RNA was used for cDNA synthesis using a cDNA synthesis kit (PrimeScript™ RT Reagent Kit with gDNA Eraser, Takara Bio, Mountain View, CA). SYBR® Premix Ex Taq™ II (Tli RNase H Plus) kit (Takara Bio) and primer sequences (Table 2) were then added to cDNA, and qRT-PCR was performed on an ABI 7500 Real-Time PCR instrument (Applied Biosystems, Thermo Fisher Scientific) with each sample run in duplicate. The threshold cycle (Ct) for endogenous control GAPDH (Ct_{GAPDH}) was subtracted from that of the gene of interest (Ct_{GOI}) obtain a ΔCt_{GOI}. Then, the $\Delta\Delta Ct_{GOI}$ was calculated by subtracting the ΔCt_{GOI} of the group 1 (control) form the ΔCt_{GOI} of the other groups (2, 3, 4, 5 and 6). The relative target

gene expression levels (i.e., Noggin and Runx2) were calculated using the $2^{-\Delta\Delta Ct}$ equation [41].

2.7. Microcomputed tomography (μCT)

To visualize and quantify bone formation after 12 weeks implantation, samples were explanted, fixed in 4% neutral buffered formalin (NBF) and then scanned using a high-resolution μCT (Skyscan 1172, Skyscan, Bruker, Belgium) with a 0.5 mm thick aluminum filter. The samples were scanned at an isotropic resolution of 10 μm, a voltage of 75 kV and current of 100 μA, a 0.5° rotation step for 360° rotation with 1110 ms acquisition time and frame averaging of 5. 3D reconstruction and analysis were performed using NRecon and CTAn software (Skyscan) with a global threshold range of 55–255. Thresholding was determined by matching the binary images with the original reconstructed images as previously described [42]. CTvox (Skyscan) was used to construct representative 3D images. The quantitative parameters bone volume fraction, trabecular number, trabecular separation, and trabecular thickness were measured in a defined cylindrical region of interest (5 mm diameter, 100 slices at 10 μm thickness = ~1 mm). The samples selected as representative μCT images (Figure 5) exhibit their BV/TV right below the average BV/TV value of corresponding groups. (N = 7 for groups 1 and 6, = 6 for groups 3 and 4, and = 5 for groups 2 and 5).

2.8. Histology

After μCT scanning, the samples were partially decalcified in Tris-EDTA buffer (2% EDTA, 0.05 M Tris-HCl (pH 7.4)) for 2 weeks, after which they were embedded in paraffin and sectioned. Five μm thick sections were deparaffinized in xylene and rehydrated in ethanol with decreasing concentrations, stained with H&E and Goldner's Trichrome and mounted with glycerol vinyl alcohol (Invitrogen). Photomicrographs of the stained sections were obtained using an Olympus BX61VS microscope (Olympus, Center Valley, PA) with a Pike F-505 camera (Allied Vision Technologies, Stadtroda, Germany). Histologic samples selected as representative were the same as those presented in the μCT results (Figure 5). Sample size is the same as that for μCT scanning above.

2.9. Statistical analysis

Quantitative data are expressed as mean ± standard deviation. Statistical analysis was performed using Tukey-Kramer Multiple Comparisons Test with one-way analysis of variance (ANOVA) using InStat software (GraphPad Software, La Jolla, CA). p values less than 0.05 were considered statistically significant.

3. Results

3.1. Polymer synthesis and hydrogel formation

Eight-arm-PEG-acrylate (8-arm-PEG-A) was synthesized via a reaction of acryloyl chloride (AC) with the hydroxyl groups of 8-arm-PEG-OH, as previously reported [20]. The degree of acrylate modification was calculated to be 85% from the NMR spectrum of 8-arm-PEG-A (Figure 1) based on the ratio of the acrylate peaks and total PEG protons. *In situ* forming PEG hydrogels were generated via Michael type reaction upon mixing 8-arm-PEG-A with

8-arm-PEG-thiol (8-arm-PEG-SH) with a 1:1 stoichiometry ratio of acrylate and thiol groups at physiological pH and room temperature [20]. A schematic of the formation of PEG hydrogels containing co-encapsulated hMSCs and RNA-polyethylenimine (PEI) nanocomplexes is presented in Figure 2. Thiolated cell adhesion peptides containing the amino acid sequence RGD (i.e., Gly-Arg-Gly-Asp-Ser-Pro-Cys or GRGDSPC) were also reacted with 8-arm-PEG-A via thiol-acrylate chemistry prior to hydrogel formation. Adhesion ligands were covalently incorporated into the PEG hydrogel network to enable attachment and survival of the encapsulated hMSCs [43–45], which are an anchorage-dependent cell population.

3.2. *In vivo* hydrogel implantation and explant PCR and biochemical analysis after 2 weeks

Previously, we reported that temporally controlled presentation of siNoggin and/or miRNA-20a to hMSCs encapsulated within the *in situ* forming PEG hydrogels enhanced their osteogenic differentiation *in vitro*. Here, to demonstrate the capacity of the hydrogel system to heal critical-sized bone defects, hMSC-encapsulated hydrogels containing a single type of RNA (i.e., siNoggin or miRNA-20a) or both RNAs together (i.e., siNoggin and miRNA-20a) were implanted into bilateral, full-thickness 5 mm calvarial bone defects in athymic rats. Six groups were investigated for *in vivo* bone formation in the rat model: Hydrogel + hMSCs (group 1 or G1), hydrogel + hMSCs + BMP-2 (G2), hydrogel + hMSCs + BMP-2 + negative control siRNA (G3), hydrogel + hMSCs + BMP-2 + siNoggin (G4), hydrogel + hMSCs + BMP-2 + miRNA20a (G5), hydrogel + hMSCs + BMP-2 + siNoggin + miRNA20a (G6) (Table 1). Osteogenesis and bone regeneration were evaluated by examining the presence of osteogenic markers 2 weeks post-implantation, and by histologic and microcomputed tomography (μCT) analysis after 12 weeks.

After two weeks, the hydrogel/hMSC constructs were explanted and assayed for early osteogenic markers alkaline phosphatase (ALP) activity and Runt-related transcription factor 2 (Runx2) and noggin expression to investigate the influence of localized and sustained delivery of siNoggin and/or miRNA-20a on the osteogenic potential of encapsulated hMSCs. At this time point, the hydrogel/hMSC constructs were easily retrievable from the defects, as they were still intact and not yet integrated with the host tissue. The sustained delivery of siNoggin with BMP-2 to hMSCs encapsulated within the hydrogels (G4) significantly downregulated noggin gene expression compared to no siRNA (G2) and the delivery of negative control siRNA (siNC; G3) at 2 weeks (Figure 3a). Noggin expression level in explants without BMP-2 (G1) was significantly lower than that in G2 and G3. Runx2 expression in G4 was also significantly higher than that in the control groups (G1-3) and the hydrogels loaded with miRNA-20a and BMP-2 (G5) (Figure 3b). Delivery of both siNoggin and miRNA-20a with BMP-2 (G6) also significantly increased Runx2 expression compared to G1. ALP activity of encapsulated hMSCs normalized to DNA content in G4 was significantly higher than all other groups except G6 (Figure 3c). In addition, G6 expressed more ALP activity than G1 and 3, and ALP activity in G5 was only higher than the G1 control (Figure 3c). Calcium content, a late osteogenic indicator, was also measured at this early time point. Calcium content normalized to DNA content in G2 was significantly higher than that in G1 and G5, and, G4 had higher calcium content than in G1 (Figure 3d).

3.3. *In vivo* bone formation after 12 weeks: μCT outcomes

After 12 weeks, the constructs were explanted for analysis via μCT and histology. Defect healing was characterized by the extent of new bone formation within the defect region. Quantitative analysis was performed to determine the 3D morphometric parameters bone volume per tissue volume (BV/TV), trabecular number (Tb.N), trabecular separation (Tb.Sp) and trabecular thickness (Tb.Th) within the defects using μCT (Figure 4). The average BV/TV of the control groups (G1-3) was 8.87, 9.21 and 12.77%, respectively, with no significant differences among these groups. The delivery of BMP-2 along with siNoggin (G4) or miRNA-20a alone (G5) or the co-delivery of siNoggin and miRNA-20a (G6) resulted in 18.88, 24.51 and 15.49% average bone volume fraction, respectively (Figure 4a). Hydrogels containing only miRNA-20a (G5) exhibited significantly higher percent bone volume compared to G1-3, and G4 produced significantly more bone than G1. Furthermore, G5 had significantly higher trabecular number than the hydrogels without RNA molecules (i.e., G1 and G2) and also lower trabecular separation than G1 (Figure 4b,c). There was no difference in trabecular thickness between any of the groups (Figure 4d). Representative 3D reconstructed μCT images reveal minimal new bone formation, primarily around the defect margins, in the control groups (G1-3) and G6, and enhanced bone regeneration in the G5 defects (Figure 5).

3.4. *In vivo* bone formation after 12 weeks: histologic outcomes

Qualitative histological analysis of the explants was performed using Hematoxylin and Eosin (H&E) and Goldner's Trichrome (GTC)-stained sections. Supplemental Figures S1 and S2 present the overall tissue composition and distribution across the defect width outlining the margins. The control groups (G1-3) exhibited limited yet relatively mature new bone (H&E: pink; GTC: turquoise) integrated with the host bone at the defect margins (Figure 6A–C,a-c1). In agreement with the μCT analysis, fibrous connective and adipose tissue devoid of significant bone was found in the central defect region for these groups (Figure 6A–C2,6a-c2). siNoggin presentation (G4) resulted in noticeably greater bone formation originating from the defect margins than the control groups (G1-3) (Figure S1 and 2). New tissue was comprised of maturing osteoid, and mixed woven and lamellar bone with lacunae-embedded osteocytes (Figure 6D,d1). Cell-rich, fibrous connective tissue with encapsulated new bone spicules was observed centrally (Figures S2D and 6D,d2). Consistent with the μCT analysis, the highest levels of bone regeneration were seen with delivery of miRNA-20a (G5). New bone was well-integrated with the host tissue at the defect margins (Figure 6E,e1), exhibiting similar overall composition as seen with G4 (Figure 6D,d1) in that area. Dual presentation of siNoggin and miRNA-20a (G6) induced similar new bone formation originating from the defect margins (Figure 6F,f1) compared to G4, but less than G5 (Figure 6E,e1). Of note, across groups new tissue in the defect center was comprised of predominantly fibrous connective tissue rendering all defects unbridged.

4. Discussion

The goal of this work was to engineer a hydrogel system for temporally controlled siRNA delivery to encapsulated and surrounding cells for repair of full-thickness rat calvarial bone defects. Previously, one study reported that a poly-D,L-lactic acid-p-dioxanone-

polyethyleneglycol block co-polymer hydrogel containing naked siNoggin and BMP-2 implanted into the dorsal muscle pouches of mice increased ectopic bone formation compared to hydrogels loaded with BMP-2 alone, but release profiles of the siRNA were not investigated, no cells were encapsulated, and bone formation was not examined at an orthotopic site [37]. Recently, a solid poly(lactic-co-glycolic acid) scaffold was used to control the release of miRNA-26a to promote bone regeneration in calvarial bone defects in a mouse model, but no cell encapsulation was presented in this work [38]. In addition, a photocrosslinked PEG hydrogel system developed for the controlled delivery of siRNA against WW domain-containing E3 ubiquitin protein ligase 1 (siWwp1) showed enhanced bone formation in murine femur fractures, but similarly, cell encapsulation was not investigated in this study [36]. A hydrogel created from four different polymers (i.e., gelatin, hyaluronic acid, PEG and heparin) was used to encapsulated hMSCs and miRNA-26a and shown to enhance bone formation in mouse calvarial bone defects compared to the delivery of hMSCs and negative control miRNA [35]. However, this hydrogel system released miRNA with initial burst release, and provided limited control over its delivery profile. Similarly, hMSC-encapsulated chitosan hydrogels containing siNoggin demonstrated enhanced bone formation in mouse calvarial defects compared to no treatment control, but no control over RNA release was demonstrated [46]. With an effort to create a cytocompatible RNA delivery system permitting tunable and controlled RNA release profiles with minimal or no initial burst release, we have developed *in situ* forming PEG hydrogels allowing for the encapsulation of viable hMSCs. By varying the density of hydrolytically degradable ester groups within the hydrogel network, siRNA release profiles were tuned and prolonged from 19 to 42 days as a result of hydrogel degradation and siRNA diffusion [20]. Building on this *in vitro* study, here we demonstrate that this hydrogel system delivering RNA and hMSCs enhanced bone formation in rat calvarial bone defects.

A critical-sized bone defect cannot heal by itself without intervention during the lifetime of the patient [47]. The delivery of stem cells using hydrogels as a cell carrier is a promising approach for regenerating lost, diseased or damaged bone tissue [48, 49]. One advantage of the use of hydrogels is that aqueous solutions of macromer precursors containing cells and/or bioactive molecules can be administered into the body via minimally invasive means, and they can then form hydrogels in situ via chemical or physical crosslinking. Several studies have shown the potential of the Michael addition reaction between an acrylate electrophile and a thiol nucleophile for making hydrogels for a wide range of biomedical applications [20, 50–54]. Certain hydrogels formed via Michael type reaction employ a toxic organic base (i.e., triethanolamine) for catalyzing thiol-acrylate polymerization [51, 52]. Here, we synthesized *in situ* forming PEG hydrogels via a thiol-acrylate addition reaction at pH 7.4 without the use of any additional chemicals that might harm cells; therefore, this chemistry is attractive for *in situ* crosslinking for tissue engineering applications utilizing cell encapsulation. PEG was chosen in this study as it is a biocompatible polymer and has been widely investigated for bone tissue engineering [55, 56]. In addition, owing to its non-ionic character, PEG presents limited interactions with positively charged RNA-PEI nanoparticles, permitting the easy regulation of RNA release via varying the density of hydrolytically degradable ester groups within the hydrogel network.

RNA interference using siRNA and miRNA has been shown to regulate stem cell signaling pathways, a valuable strategy for directing stem cell behaviors for tissue regeneration applications [19, 20, 57]. Noggin is a BMP antagonist that prevents BMPs from binding to their cognate receptors [58], leading to the downregulation of BMP-2-induced osteogenesis. With this important function, siRNA-mediated inhibition of noggin expression has been reported to increase the osteogenic differentiation of mouse osteoblasts [59], mouse adipose derived MSCs [57], C2C12 cells, a myoblastic cell line [60], mouse preosteoblasts [59] and hMSCs [20, 45, 61]. Moreover, suppression of noggin expression in mouse primary calvarial osteoblasts increased *in vivo* bone formation in mouse calvarial defects [59], and local delivery of siNoggin induced ectopic bone formation in rats [37]. In addition to siNoggin, miRNA-20a has a positive effect on hMSC osteogenic differentiation by inhibiting the expression of PPAR-γ, a down regulator of BMP signaling in osteogenesis [34, 62]. We previously reported that the *in situ* forming PEG hydrogels permitted prolonged siRNA release over 42 days. When the ester groups within the hydrogel networks hydrolytically degraded, their effective mesh size increased facilitating the diffusion of encapsulated siRNA/PEI nanoparticles out of the hydrogels. Using this system, it was demonstrated that the delivery of siNoggin and co-delivery of siNoggin and miRNA-20a from this system significantly enhanced *in vitro* osteogenic differentiation of encapsulated hMSCs compared to a non-targeting control siRNA group, while miRNA-20a alone showed minimal upregulation of stem cell osteogenic differentiation [20]. This study provided evidence that siNoggin had a strong effect on the osteogenic differentiation of encapsulated hMSCs compared to miRNA-20a in this system *in vitro*.

Here, we investigated whether the delivery of siNoggin and/or miRNA-20a enhanced bone regeneration in bilateral rat calvarial defects compared to the delivery of no siRNA or negative control siRNA using this in situ forming PEG hydrogel system with encapsulated hMSCs and BMP-2. Rat calvarial bone defects provide a highly reproducible, economical and clinically relevant *in vivo* model for evaluating bone regeneration [1]. Since noggin prevents BMP-2 from binding to its receptors on the cell surface and a target of miRNA-20a, PPAR-γ, is a negative regulator of BMP signaling, BMP-2 was co-encapsulated within hydrogel constructs along with RNA interfering molecules and hMSCs. Two weeks post-implantation, the hydrogels were explanted and the expression of noggin and Runx2 was analyzed. G2 and G3 exhibited higher noggin expression than G1, likely due to the presence of BMP-2 in G2 and G3. Previous research has reported that noggin expression in hMSCs [63] and rat osteoblasts [64] was markedly upregulated in response to BMP-2. Noggin expression in G4 was significantly lower than that in G2 and G3 indicating the strong silencing effect of siNoggin being delivered using the hydrogels. G5 and G6 have slightly lower average noggin expression than G2 and G3, but the difference was not significant. Noggin in G6 was higher than G4 as the incorporated siNoggin was only half of that in G4. As the effect of siNoggin delivery in G4, G4 expressed more Runx2, a critical early osteogenic differentiation marker, than G1-3. Runx2 expression in G6 was only higher than G1 as G6 contained half of the siNoggin as present in G4. These siNoggin and Runx2 PCR results suggest that an increased siNoggin amount loaded into the hydrogels decreased noggin and increased Runx2 expression in the encapsulated cells, which could drive hMSC osteogenic differentiation *in vivo* and potentially bone formation. G1 also presented lowest

ALP activity, likely resulting from the absence of BMP-2 in this group. The delivery of siNoggin in G4 significantly increased ALP activity compared to the control groups (G1-3) and also G5 at 2 weeks time point. G6 also produced more ALP than G1 and G3, potentially due to the effect of siNoggin. Surprisingly, miRNA-20a in G5 did not exhibit increased ALP activity compared to G2 and G3 controls by two weeks. While calcium content in G2 and G4 were higher than the G1 and G2 had more calcium than G5, the calcium contents of G4-6 were not higher than that of G2 and 3 controls at 2 weeks post-implantation, likely because it was too early for substantial mineralization to occur.

After 12 weeks implantation, bone formation in the calvarial defects was analyzed via μCT imaging (Figure 5). Control groups G1-3 exhibited limited bone formation after 12 weeks. While BMP-2 was encapsulated within the PEG hydrogels of G2-3, BMP-2 may have diffused rapidly from these hydrogels due to limited interactions between BMP-2 and the neutral PEG hydrogels, leading to little bone formation in these groups. In contrast, BMP-2 containing hydrogels encapsulated with miRNA-20a alone induced significantly more bone formation than the groups without RNA or with siNC (G1-3). However, in our previous *in vitro* report, miRNA-20a alone had little effect on calcium deposition by 4 weeks, compared to siNoggin and contransfection of siNoggin and miRNA-20a [20]. The conflicting results from these studies are likely due to the differences between *in vitro* and *in vivo* environments, leading to the inconsistency in translating *in vitro* results into *in vivo* therapies [65]. However, no bridging was observed in any group. It is likely that transplanted and host cells contributed to the bone repair. The transplanted hMSCs may have directly differentiated into chondrocytes or osteoblasts, and participated in the osteogenic process, or they could have secreted trophic signals recruiting and influencing surrounding host cells. Moreover, released BMP-2, which has been shown to induce chemotaxis of cells [66], may have stimulated host cells and aided bone repair process. Since PEG does not have an any affinity with the small BMP-2 protein, the release of BMP-2 from the hydrogels used in this study was likely completed within few days due to rapid diffusion out of the water-swollen network of PEG hydrogels [67]. The release of BMP-2 could be more sustained to prolong the influence of this osteogenic signal by, for example, coupling heparin, which has a binding affinity with BMP-2, onto the backbone of the hydrogels [68]. To further enhance bone formation *in vivo*, future studies may also focus on investigating the influence of hydrogel degradation rate *in vivo*, siRNA concentration and cell density, particularly higher siRNA, miRNA and cell concentrations, on promoting the healing of calvarial defects.

5. Conclusion

In situ forming PEG hydrogels have been engineered for localized and sustained delivery of RNAi molecules to encapsulated hMSCs, resulting in increased bone formation in a rat calvarial defect model. Specifically, presentation of miRNA-20a to hMSCs using the PEG hydrogel delivery system enhanced bone regeneration in rat calvarial defects. This biomaterial system is a promising platform for localized, sustained gene delivery for a variety of applications in tissue engineering and regenerative medicine.

Supplementary Material

Refer to Web version on PubMed Central for supplementary material.

Acknowledgments

The authors gratefully acknowledge funding from the National Institutes of Health's National Institute of Arthritis And Musculoskeletal And Skin Diseases under award numbers R01AR069564 (EA), R01AR066193 (EA) and T32AR007505 (OJ), and the National Institute of Dental & Craniofacial Research under award number R56DE022376 (EA) and F32DE024712 (SH). The contents of this publication are solely the responsibility of the authors and do not necessarily represent the official views of the National Institutes of Health.

References

1. Spicer PP, Kretlow JD, Young S, Jansen JA, Kasper FK, Mikos AG. Evaluation of bone regeneration using the rat critical size calvarial defect. Nat Protoc. 2012; 7(10):1918–1929. [PubMed: 23018195]
2. Blokhuis TJ, Arts JJC. Bioactive and osteoinductive bone graft substitutes: Definitions, facts and myths. Injury. 2011; 42:S26–S29. [PubMed: 21714968]
3. Moore WR, Graves SE, Bain GI. Synthetic bone graft substitutes. ANZ J Surg. 2001; 71(6):354–361. [PubMed: 11409021]
4. Blokhuis TJ, Arts JJC. Bioactive and osteoinductive bone graft substitutes: Definitions, facts and myths. Injury. 2011; 42(Supplement 2)(0):S26–S29. [PubMed: 21714968]
5. Nandi S, Roy S, Mukherjee P, Kundu B, De D, Basu D. Orthopaedic applications of bone graft & graft substitutes: a review. Indian J Med Res. 2010; 132:15–30. [PubMed: 20693585]
6. Habal MB, Reddi AH. Bone grafts and bone induction substitutes. Clin Plast Surg. 1994; 21(4):525–42. [PubMed: 7813153]
7. Meijer GJ, de Bruijn JD, Koole R, van Blitterswijk CA. Cell-Based Bone Tissue Engineering. PLoS Med. 2007; 4(2):e9. [PubMed: 17311467]
8. Weinand C, Pomerantseva I, Neville CM, Gupta R, Weinberg E, Madisch I, Shapiro F, Abukawa H, Troulis MJ, Vacanti JP. Hydrogel-β-TCP scaffolds and stem cells for tissue engineering bone. Bone. 2006; 38(4):555–563. [PubMed: 16376162]
9. Nguyen TBL, Lee B-T. A Combination of Biphasic Calcium Phosphate Scaffold with Hyaluronic Acid-Gelatin Hydrogel as a New Tool for Bone Regeneration. Tissue Eng Part A. 2014; 20(13–14): 1993–2004. [PubMed: 24517159]
10. Jeon O, Wolfson DW, Alsberg E. In-Situ Formation of Growth-Factor-Loaded Coacervate Microparticle-Embedded Hydrogels for Directing Encapsulated Stem Cell Fate. Adv Mater. 2015; 27(13):2216–2223. [PubMed: 25708428]
11. Jaiswal RK, Jaiswal N, Bruder SP, Mbalaviele G, Marshak DR, Pittenger MF. Adult Human Mesenchymal Stem Cell Differentiation to the Osteogenic or Adipogenic Lineage Is Regulated by Mitogen-activated Protein Kinase. J Biol Chem. 2000; 275(13):9645–9652. [PubMed: 10734116]
12. Yilgor P, Sousa RA, Reis RL, Hasirci N, Hasirci V. Effect of scaffold architecture and BMP-2/BMP-7 delivery on in vitro bone regeneration. J Mater Sci Mater Med. 2010; 21(11):2999–3008. [PubMed: 20740306]
13. Lee SS, Huang BJ, Kaltz SR, Sur S, Newcomb CJ, Stock SR, Shah RN, Stupp SI. Bone regeneration with low dose BMP-2 amplified by biomimetic supramolecular nanofibers within collagen scaffolds. Biomaterials. 2013; 34(2):452–459. [PubMed: 23099062]
14. Ruhé PQ, Boerman OC, Russel FGM, Mikos AG, Spauwen PHM, Jansen JA. In vivo release of rhBMP-2 loaded porous calcium phosphate cement pretreated with albumin. J Mater Sci Mater Med. 2006; 17(10):919. [PubMed: 16977389]
15. Carragee EJ, Hurwitz EL, Weiner BK. A critical review of recombinant human bone morphogenetic protein-2 trials in spinal surgery: emerging safety concerns and lessons learned. Spine J. 2011; 11(6):471–491. [PubMed: 21729796]
16. Blackwood KA, Bock N, Dargaville TR, Ann Woodruff M. Scaffolds for Growth Factor Delivery as Applied to Bone Tissue Engineering. Int J Polym Sci. 2012; 2012:25.

17. Wegman F, van der Helm Y, Öner FC, Dhert WJA, Alblas J. Bone Morphogenetic Protein-2 Plasmid DNA as a Substitute for Bone Morphogenetic Protein-2 Protein in Bone Tissue Engineering. Tissue Eng Part A. 2013; 19(23–24):2686–2692. [PubMed: 23901942]
18. Huang YC, Simmons C, Kaigler D, Rice KG, Mooney DJ. Bone regeneration in a rat cranial defect with delivery of PEI-condensed plasmid DNA encoding for bone morphogenetic protein-4 (BMP-4). Gene Ther. 2005; 12(5):418–426. [PubMed: 15647766]
19. Kwong FNK, Richardson SM, Evans CH. Chordin knockdown enhances the osteogenic differentiation of human mesenchymal stem cells. Arthritis Res Ther. 2008; 10(3)
20. Nguyen MK, Jeon O, Krebs MD, Schapira D, Alsberg E. Sustained localized presentation of RNA interfering molecules from in situ forming hydrogels to guide stem cell osteogenic differentiation. Biomaterials. 2014; 35(24):6278–6286. [PubMed: 24831973]
21. Smith DS, Winn S, Ozaki W, Wax MK. Bone regeneration in rats with BMP-4 and VEGF plasmid DNA. Otolaryngology - Head and Neck Surgery. 2004; 131(2):P118.
22. Luo D, Saltzman WM. Synthetic DNA delivery systems. Nat Biotech. 2000; 18(1):33–37.
23. Youn H, Chung J-K. Modified mRNA as an alternative to plasmid DNA (pDNA) for transcript replacement and vaccination therapy. Expert Opin Biol Ther. 2015; 15(9):1337–1348. [PubMed: 26125492]
24. Krebs MD, Alsberg E. Localized, targeted, and sustained siRNA delivery. Chemistry. 2011; 17(11): 3054–62. [PubMed: 21341332]
25. Presumey J, Salzano G, Courties G, Shires M, Ponchel F, Jorgensen C, Apparailly F, De Rosa G. PLGA microspheres encapsulating siRNA anti-TNFalpha: efficient RNAi-mediated treatment of arthritic joints. Eur J Pharm Biopharm. 2012; 82(3):457–64. [PubMed: 22922428]
26. Nelson CE, Kim AJ, Adolph EJ, Gupta MK, Yu F, Hocking KM, Davidson JM, Guelcher SA, Duvall CL. Tunable Delivery of siRNA from a Biodegradable Scaffold to Promote Angiogenesis In Vivo. Adv Mater. 2014; 26(4):607–614. [PubMed: 24338842]
27. Rujitanaroj P-oWang Y-C, Wang J, Chew SY. Nanofiber-mediated controlled release of siRNA complexes for long term gene-silencing applications. Biomaterials. 2011; 32(25):5915–5923. [PubMed: 21596430]
28. Cao H, Jiang X, Chai C, Chew SY. RNA interference by nanofiber-based siRNA delivery system. J Control Release. 2010; 144(2):203–212. [PubMed: 20138939]
29. Nguyen K, Dang PN, Alsberg E. Functionalized, biodegradable hydrogels for control over sustained and localized siRNA delivery to incorporated and surrounding cells. Acta Biomater. 2013; 9(1):4487–4495. [PubMed: 22902819]
30. Krebs MD, Jeon O, Alsberg E. Localized and Sustained Delivery of Silencing RNA from Macroscopic Biopolymer Hydrogels. J Am Chem Soc. 2009; 131(26):9204–9206. [PubMed: 19530653]
31. Hill MC, Nguyen MK, Jeon O, Alsberg E. Spatial Control of Cell Gene Expression by siRNA Gradients in Biodegradable Hydrogels. Adv Healthc Mater. 2015; 4(5):714–722. [PubMed: 25530099]
32. Han HD, Mora EM, Roh JW, Nishimura M, Lee SJ, Stone RL, Bar-Eli M, Lopez-Berestein G, Sood AK. Chitosan hydrogel for localized gene silencing. Cancer Biol Ther. 2011; 11(9):839–845. [PubMed: 21358280]
33. Aspenberg P, Jeppsson C, Economides AN. The bone morphogenetic proteins antagonist Noggin inhibits membranous ossification. J Bone Miner Res. 2001; 16(3):497–500. [PubMed: 11277267]
34. Zhang JF, Fu WM, He ML, Xie WD, Lv Q, Wan G, Li G, Wang H, Lu G, Hu X, Jiang S, Li JN, Lin MC, Zhang YO, Kung HF. MiRNA-20a promotes osteogenic differentiation of human mesenchymal stem cells by co-regulating BMP signaling. RNA Biol. 2011; 8(5):829–38. [PubMed: 21743293]
35. Li Y, Fan L, Liu S, Liu W, Zhang H, Zhou T, Wu D, Yang P, Shen L, Chen J, Jin Y. The promotion of bone regeneration through positive regulation of angiogenic–osteogenic coupling using microRNA-26a. Biomaterials. 2013; 34(21):5048–5058. [PubMed: 23578559]
36. Wang Y, Malcolm DW, Benoit DSW. Controlled and sustained delivery of siRNA/NPs from hydrogels expedites bone fracture healing. Biomaterials. 2017; 139:127–138. [PubMed: 28601703]

37. Manaka T, Suzuki A, Takayama K, Imai Y, Nakamura H, Takaoka K. Local delivery of siRNA using a biodegradable polymer application to enhance BMP-induced bone formation. Biomaterials. 2011; 32(36):9642–9648. [PubMed: 21963281]
38. Zhang X, Li Y, Chen YE, Chen J, Ma PX. Cell-free 3D scaffold with two-stage delivery of miRNA-26a to regenerate critical-sized bone defects. Nat Commun. 2016; 7:10376. [PubMed: 26765931]
39. Kretlow JD, Klouda L, Mikos AG. Injectable matrices and scaffolds for drug delivery in tissue engineering. Adv Drug Deliv Rev. 2007; 59(4–5):263–273. [PubMed: 17507111]
40. Sabokbar A, Millett PJ, Myer B, Rushton N. A rapid, quantitative assay for measuring alkaline phosphatase activity in osteoblastic cells in vitro. Bone Miner. 1994; 27(1):57–67. [PubMed: 7849547]
41. Livak KJ, Schmittgen TD. Analysis of Relative Gene Expression Data Using Real-Time Quantitative PCR and the 2 −ΔΔCT Method. Methods. 2001; 25(4):402–408. [PubMed: 11846609]
42. Bouxsein ML, Boyd SK, Christiansen BA, Guldberg RE, Jepsen KJ, Müller R. Guidelines for assessment of bone microstructure in rodents using micro–computed tomography. J Bone Mine Res. 2010; 25(7):1468–1486.
43. Salinas CN, Anseth KS. The influence of the RGD peptide motif and its contextual presentation in PEG gels on human mesenchymal stem cell viability. J Tissue Eng Regen Med. 2008; 2(5):296–304. [PubMed: 18512265]
44. Jeon O, Alsberg E. Photofunctionalization of alginate hydrogels to promote adhesion and proliferation of human mesenchymal stem cells. Tissue Eng Part A. 2013; 19(11–12):1424–32. [PubMed: 23327676]
45. Nguyen MK, McMillan A, Huynh CT, Schapira DS, Alsberg E. Photocrosslinkable biodegradable hydrogels with controlled cell adhesivity for prolonged siRNA delivery to hMSCs to enhance their osteogenic differentiation. J Mater Chem B. 2017; 5(3):485–495. [PubMed: 28652917]
46. Cui Z-K, Sun JA, Baljon JJ, Fan J, Kim S, Wu BM, Aghaloo T, Lee M. Simultaneous delivery of hydrophobic small molecules and siRNA using Sterosomes to direct mesenchymal stem cell differentiation for bone repair. Acta Biomater. 2017; 58:214–224. [PubMed: 28578107]
47. Cameron JA, Milner DJ, Lee JS, Cheng J, Fang NX, Jasiuk IM. Employing the biology of successful fracture repair to heal critical size bone defects. Curr Top Microbiol Immunol. 2013; 367:113–32. [PubMed: 23239235]
48. Huebsch N, Lippens E, Lee K, Mehta M, Koshy ST, Darnell MC, Desai RM, Madl CM, Xu M, Zhao X, Chaudhuri O, Verbeke C, Kim WS, Alim K, Mammoto A, Ingber DE, Duda GN, Mooney DJ. Matrix elasticity of void-forming hydrogels controls transplanted-stem-cell-mediated bone formation. Nat Mater. 2015
49. Kim HK, Shim WS, Kim SE, Lee KH, Kang E, Kim JH, Kim K, Kwon IC, Lee DS. Injectable in situ-forming pH/thermo-sensitive hydrogel for bone tissue engineering. Tissue Eng Part A. 2009; 15(4):923–33. [PubMed: 19061427]
50. Chan JW, Hoyle CE, Lowe AB, Bowman M. Nucleophile-Initiated Thiol-Michael Reactions: Effect of Organocatalyst, Thiol, and Ene. Macromolecules. 2010; 43(15):6381–6388.
51. Zustiak SP, Leach JB. Hydrolytically Degradable Poly(Ethylene Glycol) Hydrogel Scaffolds with Tunable Degradation and Mechanical Properties. Biomacromolecules. 2010; 11(5):1348–1357. [PubMed: 20355705]
52. Zustiak SP, Leach JB. Characterization of protein release from hydrolytically degradable poly(ethylene glycol) hydrogels. Biotechnol Bioeng. 2011; 108(1):197–206. [PubMed: 20803477]
53. Pritchard CD, O'Shea TM, Siegwart DJ, Calo E, Anderson DG, Reynolds FM, Thomas JA, Slotkin JR, Woodard EJ, Langer R. An injectable thiol-acrylate poly(ethylene glycol) hydrogel for sustained release of methylprednisolone sodium succinate. Biomaterials. 2011; 32(2):587–597. [PubMed: 20880573]
54. Hoffman AS. Hydrogels for biomedical applications. Adv Drug Deliv Rev. 2002; 54(1):3–12. [PubMed: 11755703]

55. Burdick JA, Anseth KS. Photoencapsulation of osteoblasts in injectable RGD-modified PEG hydrogels for bone tissue engineering. Biomaterials. 2002; 23(22):4315–4323. [PubMed: 12219821]
56. Gao G, Yonezawa T, Hubbell K, Dai G, Cui X. Inkjet-bioprinted acrylated peptides and PEG hydrogel with human mesenchymal stem cells promote robust bone and cartilage formation with minimal printhead clogging. Biotechnol J. 2015; 10(10):1568–1577. [PubMed: 25641582]
57. Cui Z-K, Fan J, Kim S, Bezouglaia O, Fartash A, Wu BM, Aghaloo T, Lee M. Delivery of siRNA via cationic Sterosomes to enhance osteogenic differentiation of mesenchymal stem cells. J Control Rel. 2015; 217:42–52.
58. Zimmerman LB, De Jesús-Escobar JM, Harland RM. The Spemann Organizer Signal noggin Binds and Inactivates Bone Morphogenetic Protein 4. Cell. 86(4):599–606. [PubMed: 8752214]
59. Wan DC, Pomerantz JH, Brunet LJ, Kim J-B, Chou YF, Wu BM, Harland R, Blau HM, Longaker MT. Noggin Suppression Enhances in Vitro Osteogenesis and Accelerates in Vivo Bone Formation. J Biol Chem. 2007; 282(36):26450–26459. [PubMed: 17609215]
60. Takayama K, Suzuki A, Manaka T, Taguchi S, Hashimoto Y, Imai Y, Wakitani S, Takaoka K. RNA interference for noggin enhances the biological activity of bone morphogenetic proteins in vivo and in vitro. J Bone Miner Metab. 2009; 27(4):402–411. [PubMed: 19252814]
61. Huynh CT, Nguyen MK, Naris M, Tonga GY, Rotello VM, Alsberg E. Light-triggered RNA release and induction of hMSC osteogenesis via photodegradable, dual-crosslinked hydrogels. Nanomedicine (Lond). 2016; 11(12):1535–50. [PubMed: 27246686]
62. Huynh CT, Zheng Z, Nguyen MK, McMillan A, Yesilbag Tonga G, Rotello VM, Alsberg E. Cytocompatible Catalyst-Free Photodegradable Hydrogels for Light-Mediated RNA Release To Induce hMSC Osteogenesis. ACS Biomater Sci Eng. 2017; 3(9):2011–2023.
63. Chen C, Uludag H, Wang ZX, Jiang HX. Noggin suppression decreases BMP-2-induced osteogenesis of human bone marrow-derived mesenchymal stem cells In Vitro. J Cell Biochem. 2012; 113(12):3672–3680. [PubMed: 22740073]
64. Gazzerro E, Gangji V, Canalis E. Bone morphogenetic proteins induce the expression of noggin, which limits their activity in cultured rat osteoblasts. J Clin Invest. 1998; 102(12):2106–2114. [PubMed: 9854046]
65. Rai B, Lin JL, Lim ZXH, Guldberg RE, Hutmacher DW, Cool SM. Differences between in vitro viability and differentiation and in vivo bone-forming efficacy of human mesenchymal stem cells cultured on PCL–TCP scaffolds. Biomaterials. 2010; 31(31):7960–7970. [PubMed: 20688388]
66. Behr B, Sorkin M, Lehnhardt M, Renda A, Longaker MT, Quarto N. A comparative analysis of the osteogenic effects of BMP-2, FGF-2, and VEGFA in a calvarial defect model. Tissue Eng Part A. 2012; 19(9–10):1079–1086.
67. Leach JB, Schmidt CE. Characterization of protein release from photocrosslinkable hyaluronic acid-polyethylene glycol hydrogel tissue engineering scaffolds. Biomaterials. 2005; 26(2):125–35. [PubMed: 15207459]
68. Jeon O, Powell C, Solorio LD, Krebs MD, Alsberg E. Affinity-based growth factor delivery using biodegradable, photocrosslinked heparin-alginate hydrogels. J Control Release. 2011; 154(3):258–66. [PubMed: 21745508]

Statement of Significance

Delivery of RNAi molecules may be a valuable strategy to guide cell behavior for tissue engineering applications, but to date there have been no reports of a biomaterial system capable of both encapsulation of cells and controlled delivery of incorporated RNA. Here, we present PEG hydrogels that form in situ via Michael type reaction, and that permit encapsulation of hMSCs and the concomitant controlled delivery of siNoggin and/or miRNA-20a. These RNAs were chosen to suppress noggin, a BMP-2 antagonist, and/or PPAR-γ, a negative regulator of BMP-2-mediated osteogenesis, and therefore promote osteogenic differentiation of hMSCs and subsequent bone repair in critical-sized rat calvarial defects. Simultaneous delivery of hMSCs and miRNA-20a enhanced repair of these defects compared to hydrogels containing hMSCs without siRNA or with negative control siRNA. This in situ forming PEG hydrogel system offers an exciting platform for healing critical-sized bone defects by localized, controlled delivery of RNAi molecules to encapsulated hMSCs and surrounding cells.

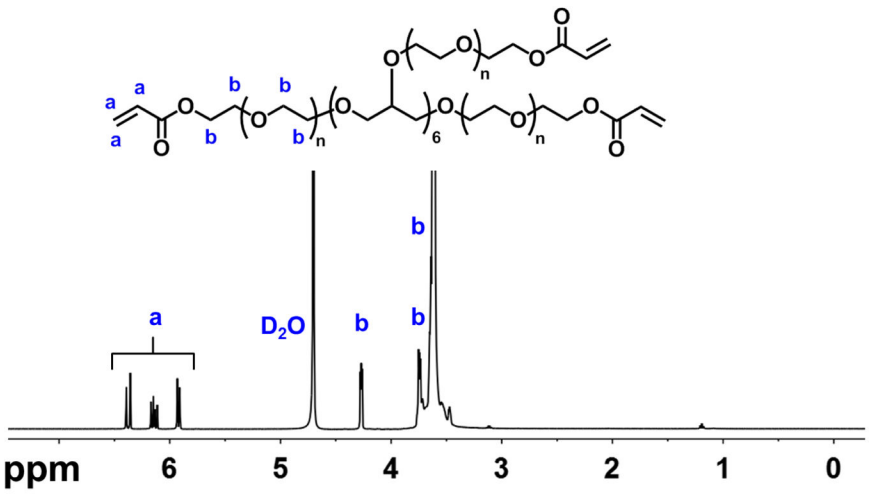

Figure 1.
Proton NMR spectrum of 8-arm-PEG-A in D_2O.

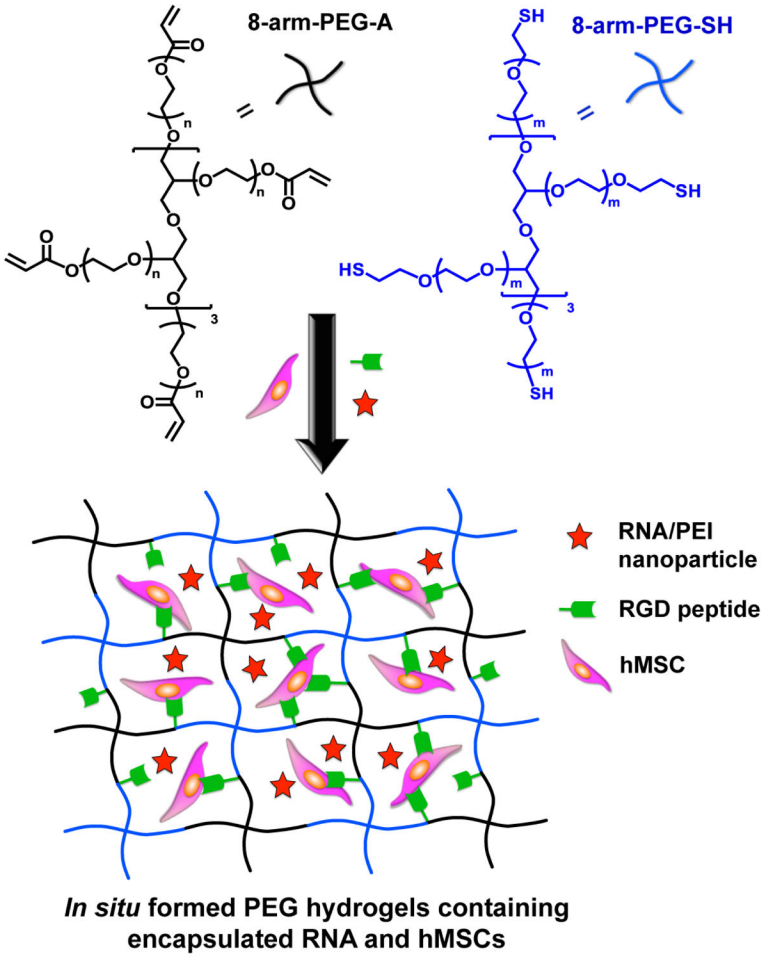

Figure 2.

Schematic of *in situ* hydrogel formation via thiol-acrylate reaction and encapsulation of RNA-PEI nanocomplexes and hMSCs.

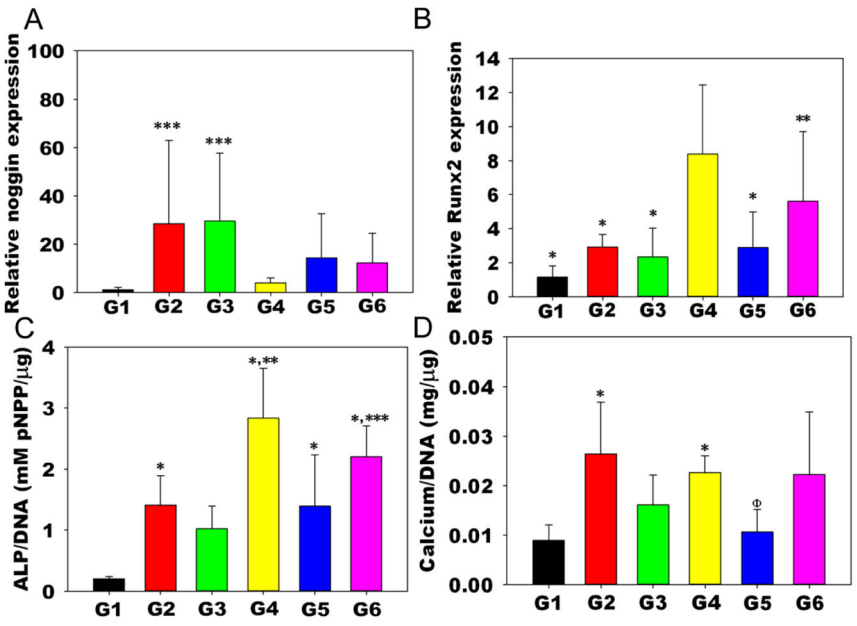

Figure 3.

Biochemical assays of the constructs 2 weeks post-implantation. A) Noggin expression $p < 0.05$ compared to ***G1 and G4; B) Runx2 expression, $p < 0.05$ compared to * G4, ** G1; C) ALP activity normalized to DNA content, $p < 0.05$ compared to *G1, **G2,3,5, ***G3; and D) Calcium normalized to DNA content, $p < 0.05$ compared to *G1, $^{\Phi}$G2.

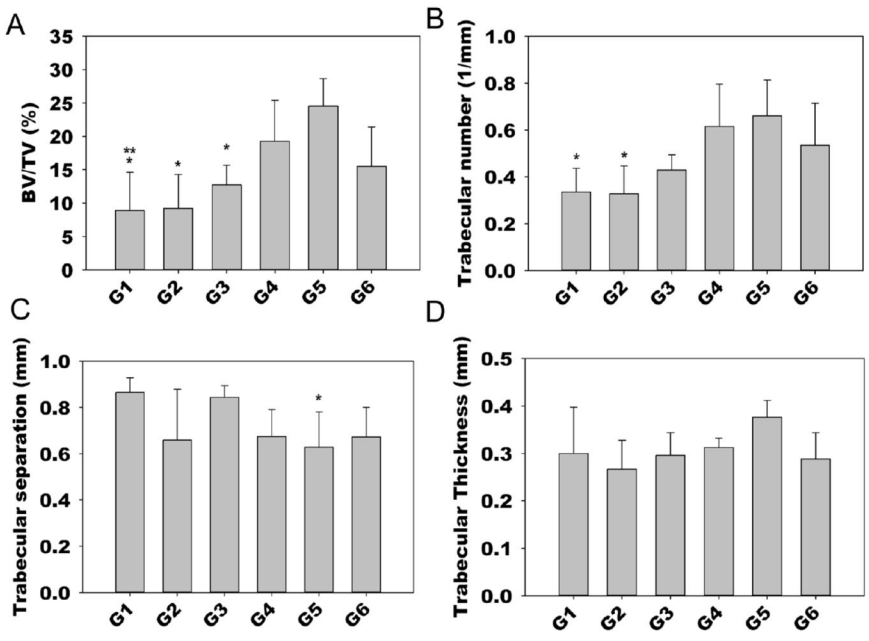

Figure 4.

Quantitative microCT analysis 12 weeks post-implantation. A) Bone volume/tissue volume (BV/TV) ($p < 0.05$ compared to * G5, ** G4), B) Trabecular number ($p < 0.05$ compared to * G5), C) Trabecular separation ($p < 0.05$ compared to * G1), and D) Trabecular thickness.

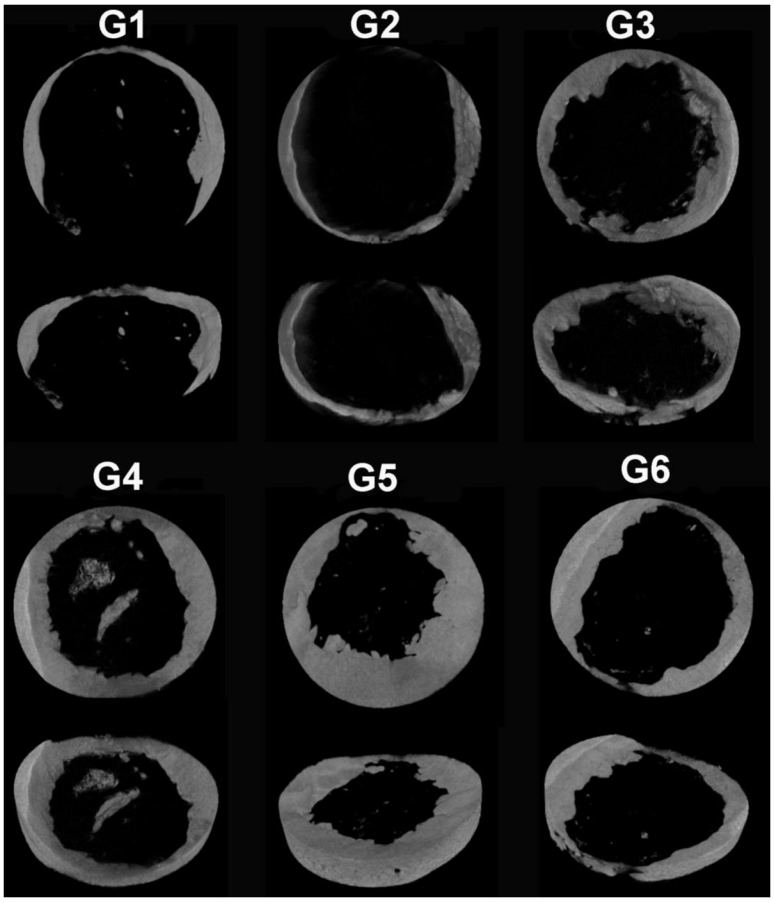

Figure 5.
Representative 3D reconstructed μCT images of the 5 mm rat calvarial bone defects 12 weeks post-implantation.

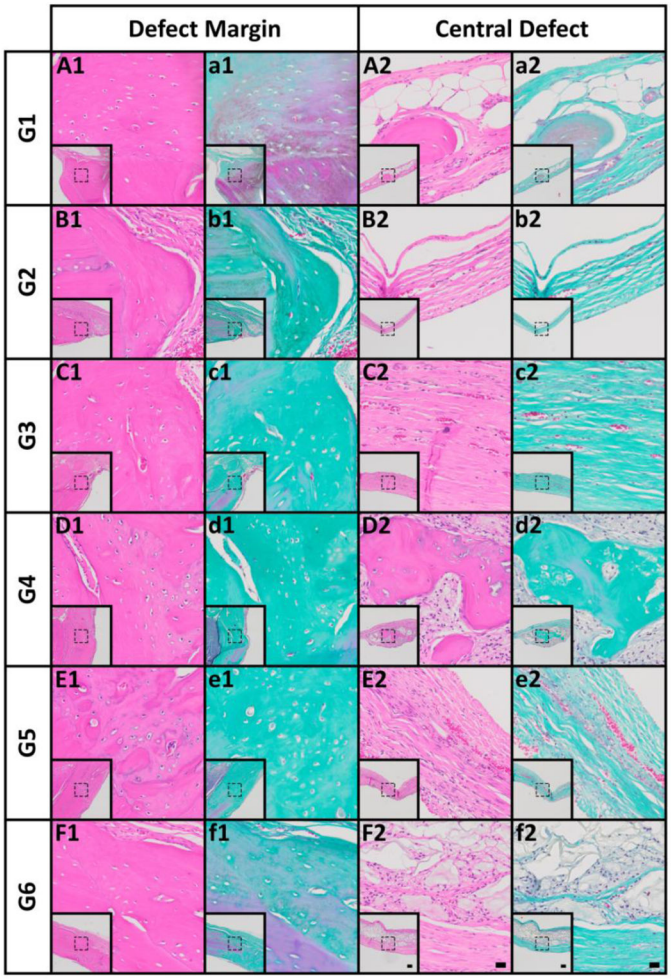

Figure 6.

Histological evaluation at 12 weeks post-implantation. (A1–F1) Photomicrographs of H&E- and (a1–f1) Goldner's trichrome-stained sections at the defect margin. (A2–F2) H&E- and (a2–f2) Goldner's trichrome-stained sections at a central region of the defect. Scale bars = 100 μm (inset), 20 μm (magnification of dotted squares).

Table 1

In vivo study experimental conditions.

Group	hMSCs (10^3 cells)	siNC (μg)	siNoggin (μg)	miRNA- 20a (μg)	siNoggin and miRNA-20a (μg)	BMP-2 (μg)
G1	170					
G2	170					1
G3	170	0.68				1
G4	170		0.68			1
G5	170			0.68		1
G6	170				0.68	1

Table 2

Primer sequences used for qRT-PCR.

Gene	Direction	Primer sequence
GAPDH	Forward	GGGGCTGGCATTGCCCTCAA
	Reverse	GGCTGGTGGTCCAGGGGTCT
noggin	Forward	CTCTAGCGAGGGTTTTCAAT
	Reverse	GTGCATTACAGGAACCAGAA
Runx2	Forward	ACAGAACCACAAGTGCGGTGCAA
	Reverse	TGGCTGGTAGTGACCTGCGGA